

Archive ouverte UNIGE

https://archive-ouverte.unige.ch

Article scientifique

Article

2020

Accepted version

Open Access

This is an author manuscript post-peer-reviewing (accepted version) of the original publication. The layout of the published version may differ .

Heteroaggregation between Charged and Neutral Particles

Trefalt, Gregor; Cao, Tianchi; Sugimoto, Takuya; Borkovec, Michal

How to cite

TREFALT, Gregor et al. Heteroaggregation between Charged and Neutral Particles. In: Langmuir, 2020, vol. 36, n° 19, p. 5303–5311. doi: 10.1021/acs.langmuir.0c00667

This publication URL: https://archive-ouverte.unige.ch/unige:136255

Publication DOI: <u>10.1021/acs.langmuir.0c00667</u>

© This document is protected by copyright. Please refer to copyright holder(s) for terms of use.

DOI: 10.1021/acs.langmuir.0c00667

Heteroaggregation between charged and neutral particles

Gregor Trefalt¹, Tianchi Cao^{1,2}, Takuya Sugimoto³, and Michal Borkovec^{1,*}

¹Department of Inorganic and Analytical Chemistry, University of Geneva, Sciences II, 30 Quai Ernest-Ansermet, 1205 Geneva, Switzerland

²Present address: Department of Chemical and Environmental Engineering, Yale University, New Haven, CT 06520, USA

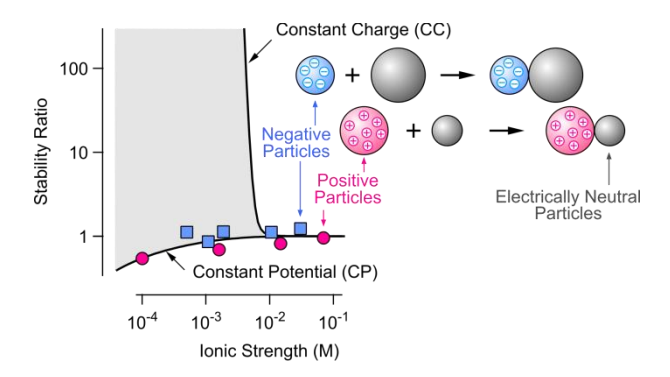
³Graduate School of Agricultural and Life Sciences, University of Tokyo, 1-1-1 Yayoi, Bunkyou-ku, Tokyo, 113-8657, Japan

*Corresponding author, Email: michal.borkovec@unige.ch

Abstract

Experimentally determined heteroaggregation rates between charged and neutral colloidal particles are reported for the first time. Different positively and negatively charged polystyrene latex particles are investigated. The neutral particles are obtained through adsorption of an appropriate amount of oppositely charged additives, such as aliphatic oligoamines, iron cyanide complexes, or alkyl sulfates. Heteroaggregation rates were measured with time-resolved multi-angle light scattering. One observes that heteroaggregation between charged and neutral particles is always fast and diffusion controlled. These experimental values are compared with calculations of the Derjaguin, Landau, Verwey, and Overbeek (DLVO) theory, whereby one finds that this heteroaggregation process is highly sensitive to charge regulation conditions. The comparison with experiments shows unambiguously that the surface of the neutral particles regulates strongly, and probably behaves close to a constant potential surface. This observation is in line with direct force measurements on similar systems, and further agrees with the fact that for neutral surfaces the capacitance of the diffuse layer is expected to be much smaller than the one of the inner layer.

Table of Contents (TOC) Graphic



Introduction

While aggregation between colloidal particles was studied for more than a century, these investigations mostly focused on homoaggregation, where the same (or very similar) colloidal particles are involved. ¹⁻¹⁰ These processes are relevant in certain applications, including ceramic processing, fabrication of paints, or drug delivery. 11-14 Various techniques are currently available to study these processes experimentally, particularly, time-resolved light scattering, turbidity measurements, or single particle counting. 14-18 Fundamental understanding of homoaggregation was already put forward with the landmark developments by Derjaguin, Landau, Verwey, and Overbeek (DLVO). 19,20,2,1 For electrically charged particles, this theory predicts two main regimes for homoaggregation, namely fast and slow aggregation. Slow aggregation occurs at low salt levels, whereby the interplay between attractive van der Waals forces and repulsive double layer forces induces an energy barrier. This barrier is surmounted by thermal activation, which leads to a slow, reaction controlled aggregation process. Fast aggregation occurs at high salt levels, where double layer forces are screened, and particles interact through attractive van der Waals forces only. Particle encounters are now dictated by diffusion, which is a fast process. In this like-charged scenario, the transition between the slow and fast regime is rather abrupt, and referred to as critical coagulation concentration (CCC). When particles undergo a charge reversal, homoaggregation features two CCCs, whereby the charge neutralization point lies in between. ^{6,8} At this point, homoaggregation is also fast, since the particles are electrically neutral, and thus the double layer interaction is equally absent.

The continuing research focus on homoaggregation may seem surprising, as many systems relevant in applications contain various types of particles. Examples where such particle mixtures are particularly important include papermaking, waste water treatment, or food processing. ²¹⁻²³ Such heteroaggreation processes, which involve different types of colloidal particles, were studied much less frequently, however. ²⁴⁻²⁷ The main reason is surely the experimental difficulty to distinguish the different aggregation processes occurring in mixed particle suspensions. Even in the early stages, where particle monomers and dimers dominate, homoaggregation and heteroaggregation may occur simultaneously, and the measurement of the corresponding heteroaggregation rates represents a major challenge. In the past, the use of different particles with similar optical response ^{28,25}, variations of the particle fractions ^{26,28,27}, or single particle counting techniques ^{29,30} were advocated to be capable to address these challenges. In our view, however, the only successful approach so far is multi-angle time-resolved light scattering. ^{15,31,32} When the respective particle pair is suitably chosen, this technique is capable to separate homoaggregation and heteroaggregation processes in the early-stages, and permits routine determination of heteroaggregation rates in a reliable fashion.

Nevertheless, heteroaggregation was studied in one special situation in some detail, namely in mixtures of oppositely charged colloidal particles. ^{25,27,31} The reason why such systems can be studied

rather easily is that only heteroaggregation occurs at lower salt levels, since both homoaggregation processes become very slow somewhat below the respective CCCs. The remaining heteroaggregation process can then be studied with analogous techniques as established for homoaggregation. These investigations conclude that in the oppositely charged scenario, heteroaggregation is fast in the whole concentration regime. In fact, it becomes even somewhat faster at low salt concentrations. When the DLVO theory is extended to this situation, the observed behavior is predicted well. The reason why heteroaggregation becomes faster with decreasing salt concentration is due to the strengthening of the attractive double layer force. However, this variation is weak, since the overall interaction forces remain attractive, and particle aggregation is governed by diffusion in the entire concentration regime. This oppositely charged heteroaggregation scenario appears rather robust with respect to modest charge asymmetries. Similarly, the like-charged heteroaggregation scenario featuring a well-defined CCC seems to tolerate modest charge asymmetries as well.

However, one important heteroaggregation scenario not studied experimentally so far is the one involving charged and neutral particles. Some of us have published a computational study based on DLVO theory of this charge-neutral case. This study suggests that this heteroaggregation process could either resemble the like-charged homoaggregation scenario featuring a slow and fast regime with a CCC in between, or the oppositely charged heteroaggregation scenario, where the aggregation remains fast in the whole concentration regime. The transition between these two scenarios appears to be dictated by the regulation characteristics of the neutral particle. For constant charge (CC) boundary conditions, the like-charged homoaggregation scenario is expected, while for constant potential (CP) conditions, the oppositely charged heteroaggregation scenario should emerge. These suggestions are most surprising, since the few studies focusing on effects of charge regulation on particle aggregation concluded that such effects are always minor. We further remark that later stages of such heteroaggregation process might show interesting features, but here we focus on early stages only.

Methods

Materials. Experiments were carried out in suspensions of spherical amidine latex (AL) and sulfate latex (SL) particles of low polydispersity. Two different types of the latter particles are used, larger SL1 particles and smaller SL2 particles. Relevant properties of these particles are summarized in Table 1. These particles were extensively purified by dialysis against pure water. Analytical grade K₃Fe(CN)₆, K₄Fe(CN)₆, and pentaethylenehexamine (N6) with the chemical formula H₂N(CH₂CH₂NH) ₄CH₂CH₂NH₂ was obtained from Sigma-Aldrich, and analytical grade sodium noctyl sulfate (OS) from Alfa Aesar. These compounds were dissolved in pure water, all solutions were adjusted to pH 4.0 with diluted HCl, and the salt level was further set by adding KCl or NaCl. MilliQ water (Millipore) was used throughout. All experiments were carried out at a temperature of 25°C.

Light scattering. Particle suspensions were characterized with static, dynamic, and electrophoretic light scattering. Electrophoretic mobility reveals that in suspensions containing monovalent ions only, the AL particles are positively charged, while the SL particles negatively. Respective measurements of the homoaggregation rate were carried out with time-resolved light scattering at a fixed angle of 90°. More details concerning the characterization of these particle suspensions are given elsewhere. 32,34

Heteroaggregation was followed by time-resolved multi-angle dynamic light scattering. 32,31 The respective mixed suspensions were investigated at high concentrations of monovalent salts, and at various concentrations of the additives. Initially, the binary colloidal suspension contains only particle monomers, denoted as A and B. To probe the aggregation process between these particles, the apparent hydrodynamic radius R(Q,t) is extracted from the second cumulant of the intensity correlation function versus the experimental time t and is further simultaneously measured for different scattering vectors. The magnitude of the scattering vector Q is related to the scattering angle θ through the relation $Q = (4\pi/\lambda)\sin(\theta/2)$, where λ is the wavelength of the light in the medium. The initial increase is of this quantity is linear, and can be expressed as the apparent dynamic rate

$$\Delta(q) = \frac{1}{R(Q,0)} \cdot \frac{dR(Q,t)}{dt} \bigg|_{t \to 0}$$
 (1)

In early stages of the aggregation, the three different particle dimers AA, AB, and BB form. As these processes occur independently, each of these dimers contributes in an additive fashion to the apparent dynamic rate as ^{31,32}

$$\Delta(Q) = k_{AA} H_{AA}(Q) + 2k_{AB} H_{AB}(Q) + k_{BB} H_{BB}(Q)$$
 (2)

where k_{ij} are the aggregation rate coefficients and $H_{ij}(Q)$ are characteristic functions that depend on the respective particle concentrations and the magnitude of the scattering vector Q. The subscripts i and j refer to the particles A and B. The particle concentrations can be conveniently expressed in terms of the total particle concentration N_0 and the number fraction of one particle type x_A or x_B , whereby $x_A + x_B = 1$. The Q-dependence arises through the scattering functions of the monomers and dimers, and the respective hydrodynamic properties. The characteristic functions can be accurately calculated through the T-matrix theory and low Reynolds number hydrodynamics for pairs of spheres. $^{32,31,35-37}$ These calculations rely on particle radii and polydispersities determined with static light scattering (see Table 1) and theoretical estimates of particle dimer diffusion coefficients. As in previous studies, we report the measured aggregation rate coefficients in terms of the stability ratio 32,31

$$W_{ij} = \frac{k_{ij}^{\text{(fast)}}}{k_{ii}} \tag{3}$$

where k_{ij} is the experimental aggregation rate coefficient, while $k_{ij}^{\text{(fast)}}$ is the same quantity at high concentrations of monovalent electrolyte.

Pressures in the plate-plate geometry. Double layer interactions between two charged plates separated with an electrolyte solution can be described with the Poisson-Boltzmann (PB) theory. This theory assumes that the electrostatic potential $\psi(x)$ in an electrolyte solution containing ions of type μ with bulk number concentrations c_{μ} of ions of type and valence z_{μ} satisfies the PB equation¹

$$\frac{d^2\psi}{dx^2} = -\frac{q}{\varepsilon_0 \varepsilon} \sum_{\mu} z_{\mu} c_{\mu} e^{-z_{\mu} \beta q \psi} \tag{4}$$

where x is the position between the plates located at $x = \pm h/2$, q is the elementary charge, ε_0 is the permittivity of vacuum, $\varepsilon = 80$ is the dielectric constant of water, and $\beta = 1/(k_{\rm B}T)$ is the inverse thermal energy, with $k_{\rm B}$ being the Boltzmann constant and T the absolute temperature. Thereby, h denotes the separation distance between the plates. This equation must be solved with respect to the boundary conditions 7,32

$$\pm \varepsilon_0 \varepsilon \frac{d\psi}{dx}\bigg|_{x=\pm h/2} = \sigma_{\pm} - C_{\rm in}^{(\pm)} [\psi(\pm h/2) - \psi_{\pm}]$$
 (5)

where σ_{\pm} , ψ_{\pm} , and $C_{\rm in}^{(\pm)}$ are the surface charge density, the diffuse layer potential, and the inner capacitance of the isolated surfaces, respectively. Thereby, + refers to the surface on the right, and – to the surface on the left. The parameters σ_{\pm} and ψ_{\pm} are connected through the PB charge-potential relationship

$$\sigma_{\pm} = \operatorname{sgn}(\psi_{\pm}) \left[2k_{\mathrm{B}} T \varepsilon_{0} \varepsilon \sum_{\mu} c_{\mu} (e^{-z_{\mu} \beta q \psi_{\pm}} - 1) \right]^{1/2}$$
(6)

where sgn(x) denotes the sign function. Note that equation (6) is only valid for the isolated surfaces. The regulation parameter of each surface is defined as^{7,32}

$$p_{\pm} = \frac{C_{\rm dl}^{(\pm)}}{C_{\rm dl}^{(\pm)} + C_{\rm in}^{(\pm)}} \tag{7}$$

where $C_{\rm dl}^{(\pm)}$ is the diffuse layer capacitance given by

$$C_{\text{dl}}^{(\pm)} = \frac{\partial \sigma_{\pm}}{\partial \psi_{\pm}} = -\operatorname{sgn}(\psi_{\pm}) \left(\frac{\beta q^{2} \varepsilon_{0} \varepsilon}{2} \right)^{1/2} \frac{\sum_{\mu} z_{\mu} c_{\mu} (e^{-z_{\mu} \beta q \psi_{\pm}} - 1)}{\left[\sum_{\mu} c_{\mu} (e^{-z_{\mu} \beta q \psi_{\pm}} - 1) \right]^{1/2}}$$
(8)

The regulation parameter assumes simple values for the boundary conditions of constant potential (CP, $p_{\pm} = 0$) and constant charge (CC, $p_{\pm} = 1$).

Once the potential profile is known, the pressure generated by the double layer is then found from ¹

$$\Pi_{\rm dl} = k_{\rm B} T \sum_{\mu} c_{\mu} \left(e^{-z_{\mu} \beta q \psi} - 1 \right) - \frac{\varepsilon_0 \varepsilon}{2} \left(\frac{d \psi}{dx} \right)^2 \tag{9}$$

The PB equation was solved in two different ways. First, this equation was solved numerically without making any further approximations. Second, we have assumed that the electric potentials were sufficiently low in magnitude, whereby the PB theory reduces to the simpler Debye-Hückel (DH) theory. In this case, the electrostatic potential can be obtained from the DH equation¹

$$\frac{d^2\psi}{dx^2} = \kappa^2 \psi \tag{10}$$

where κ is the inverse Debye length and is given by

$$\kappa^2 = \frac{2q^2I}{k_{\rm B}T\varepsilon_0\varepsilon} \tag{11}$$

where the ionic strength expressed as number concentration is

$$I = \frac{1}{2} \sum_{\mu} z_{\mu}^{2} c_{\mu} \tag{12}$$

The charge-potential relationship given in eq. (6) simplifies within the DH theory to

$$\sigma_{+} = \varepsilon_{0} \varepsilon \kappa \psi_{+} \tag{13}$$

and the diffuse capacitance given by eq. (8) to

$$C_{\rm dl}^{(\pm)} = \varepsilon_0 \varepsilon \kappa \tag{14}$$

In the charged-neutral case, we assume that the plate on the right had side is charged and the one on the left hand side is neutral, and thus $\sigma_+ \neq 0$ and $\sigma_- = 0$. In this situation, the pressure between the two plates becomes 38,33

$$\Pi_{\rm dl}(h) = \frac{2\sigma_+^2}{\varepsilon_0 \varepsilon} \cdot \frac{(2p_- - 1)e^{-2\kappa h}}{\left[1 + (2p_+ - 1)(2p_- - 1)e^{-2\kappa h}\right]^2}$$
(15)

DLVO theory suggests that the overall pressure $\Pi_{\rm vdW}(h)$, which depends on the separation distance h, has two contributions. The first is the contribution from the double layer $\Pi_{\rm dl}(h)$, and the second is the van der Waals pressure $\Pi_{\rm vdW}(h)$, namely¹

$$\Pi(h) = \Pi_{dl}(h) + \Pi_{vdW}(h) \tag{16}$$

The van der Waals pressure is calculated from the non-retarded model

$$\Pi_{\text{vdW}}(h) = -\frac{H}{6\pi} \cdot \frac{1}{h^3} \tag{17}$$

where H is the Hamaker constant. This constant is assumed to be independent on the surface charge.

Calculation of particle aggregation rate coefficients. To obtain the aggregation rates for a given particle pair i and j, one must first know the interaction potential acting between these particles. This quantity can be obtained by means of the Derjaguin approximation. In particular, knowing the overall pressure acting between the two walls, a double integration leads to the interaction potential

$$V_{ij}(h) = \pi \rho_{ij} \int_{h}^{\infty} \prod_{h'} \Pi(h'') dh'' dh'$$
(18)

where the abbreviation ρ_{ij} is given by $2\rho_{ij}^{-1} = R_i^{-1} + R_j^{-1}$, whereby R_i is the particle radius, and $\Pi(h)$ is the pressure acting between the two walls of identical material and surface properties as the particles in question. The aggregation rate coefficients can be calculated from the relation^{1,31}

$$k_{ij} = \frac{4}{3\beta\eta\rho_{ij}} \left[\int_{0}^{\infty} \frac{B_{ij}(h)e^{\beta V_{ij}(h)}}{(R_i + R_j + h)^2} dh \right]^{-1}$$
(19)

where $V_{ij}(h)$ is the interaction potential between the particles, $\eta = 8.9 \times 10^{-4}$ Pas is the shear viscosity of water, and the hydrodynamic resistance function is¹

$$B_{ij}(h) = \frac{6h^2 + 13\rho_{ij}h + 2\rho_{ij}^2}{6h^2 + 4\rho_{ij}h}$$
 (20)

Finally, the stability ratios are calculated from eq. (3) where $k_{ij}^{\text{(fast)}}$ is obtained by considering van der Waals forces only.

Results and Discussion

This study presents experimental data for heteroaggregation in the charged-neutral case for the first time. Comparison of these measurements with DLVO theory demonstrates that the neutral particles must regulate close to CP conditions. These findings are based on a reanalysis of the original experimental data, which were published recently.^{32,34} However, the corresponding datasets were published in a fashion, which is not very useful for the present analysis. Therefore, we describe the

additional steps necessary to obtain the heteroaggregation rates in the charged-neutral case. We further demonstrate that systems that are chemically completely different behave in a very similar way. For completeness, the necessary experimental techniques are also summarized.

Experimental results. Spherical and monodiperse polystyrene latex particles of different surface functionalities particles were used in these experiments, see Table 1. When suspended in solutions of simple monovalent electrolytes, the amidine particles (AL) acquire a positive charge, while the two types of sulfate particles (SL1 and SL2) investigated a negative one. Either of these particles can be made electrically neutral with a strongly adsorbing oppositely charged additive. One useful cationic additive is the aliphatic polyamine, pentaethylenehexamine (N6), which was used to neutralize SL1 particles. The respective electrophoretic mobility is shown in the right panel of Fig. 1a. At low N6 concentration, the SL1 particles are negatively charged, as suggested by the negative mobility. With increasing N6 concentration, the mobility increases to positive values, and passes though zero at a concentration around $0.70\pm0.05~\mu\text{M}$ (arrow). At this charge reversal point, the SL1 particles are electrically neutral. At the same time, the AL particles remain positively charged, as evident from the mobility measurements shown in the left panel of Fig 1a. The same situation persists in the presence of added monovalent salt, whereby the charge reversal point shifts for the SL1 particles towards higher N6 concentrations, see arrows in Fig. 1a. As evidenced by electrophoresis, the AL particles always remain positively charged under these conditions.

Similar kind of charged-neutral particle pairs can also be realized with anionic additives. Short-chain anionic surfactant sodium n-octyl sulfate (OS) were used with together with AL and SL2 particles. As illustrated in Fig. 1b, OS reverses the charge of the SL2 particles and the charge neutralization points are situated at concentrations near 0.5 ± 0.1 mM. In contrast to the N6 system discussed above, the charge neutralization point shifts only slightly upon the addition of monovalent salt. This different sensitivity to the presence of salt suggests that the adsorption of the surfactants is governed by hydrophobic interactions, while the adsorption of N6 is mainly due to electrostatic forces. For the particle pair AL and SL1, the charge of the AL particles can be also neutralized with $K_3Fe(CN)_6$ or $K_4Fe(CN)_6$, see Fig. 1c. The charge neutralization occurs at 0.30 ± 0.06 mM and 0.10 ± 0.01 mM, respectively. The charge reversal in the presence of the latter salt occurs at lower concentrations, since the $Fe(CN)_6^{4-}$ anion adsorbs to the oppositely charged AL particle surface more strongly than the $Fe(CN)_6^{3-}$ anion. In the presence of all anionic additives used, the SL1 and SL2 particles remain negatively charged, as expected. The concentrations of the additives at the charge reversal point are summarized in Table 2 for all systems investigated.

Consider now the time-resolved multi-angle dynamic light scattering measurements of the aggregation rate coefficients in the early stages in mixed suspensions containing two types of particles. The rate coefficients can be extracted by measuring the apparent dynamic rate versus the different scattering

vectors Q. Representative results are shown in Fig. 2. Consider first the situation at high concentration of monovalent salt shown in the left column in Fig. 2. In this situation, all three dimers form at comparable rates. The rate coefficient k_{AB} can be extracted from the data shown by fitting eq. (2). The homoaggreation rate coefficients k_{AA} and k_{BB} are not fitted, since their values were independently determined in homoaggregation experiments in respective suspensions containing only one particle type. Fast homoaggregation rates were measured in the same suspensions with time-resolved multi-angle dynamic light scattering at high salt concentrations, see Table 1. The fast heteroaggregation rates are given in the caption of Fig. 2, and they are close to the values for homoaggregation given in Table 1.

Similar light scattering measurements were carried out in the presence of the different additives near the charge neutralization point, and typical results are shown in the right column of Fig. 2. The results for N6 are shown in Fig. 2a, those for OS in Fig. 2b, and those for K₃Fe(CN)₆ in Fig. 2c. As evidenced by the appearance of zero lines in the figures, one of the homoaggreagtion processes does not occur, since the respective particles are highly charged. The heteroaggregation rate coefficient can be reliably extracted by fitting the observed apparent dynamic rate to eq. (2). Thereby, the homoaggregation rate coefficient was fixed again during the fit as it was determined by means of independent experiments in suspensions containing the AL particles only.

The measured stability ratios for heteroaggregation and for homoaggregation versus the concentration of the additives are reported in Fig. 3. The results for N6 and OS with and without added monovalent salt are shown in Fig. 3a,b, respectively, and those for $K_3Fe(CN)_6$ and $K_4Fe(CN)_6$ in Fig. 3c. Under these conditions, the homoaggregation process involving the highly charged particles does not occur.

In spite of the different chemical nature of the systems investigated, Fig. 3 shows that the dependencies of the stability ratios on the concentration of the additives are similar. For homoaggregation, this ratio goes through a broad minimum, which is situated around the charge reversal point, and is delimited by two CCCs on each side. For heteroaggregation, this ratio is below one at low concentrations, but increases strongly when the concentration exceeds the one at the charge reversal point. Heteroaggregation stability ratios for the charged-neutral case were obtained by interpolating the respective stability ratios, and by extracting their values at the charge reversal point. The same interpolations were carried out for different monovalent salt concentrations in the N6 and OS systems, some of which are shown in Fig. 3a,b.

The resulting stability ratios involving heteroaggregation between charged and neutral particles are plotted versus the solution ionic strength in Fig. 4. The corresponding numerical values are also given in Table 2. For all systems investigated, the stability ratios are close to unity. These ratios also

decrease with decreasing ionic strength somewhat. Heteroaggregation between charged and neutral particles thus always seems to be fast.

DLVO calculations. Let us now compare these results with calculations of the stability ratio for heteroaggregation between charged and neutral particles based on DLVO theory. While the classical superposition approximation suggests that double layer forces between a charged and a neutral surface vanish, a more detailed analysis of this situation reveals that these forces are also present. This effect is best illustrated with the simple exponential Debye-Hückel (DH) law for the osmotic pressure acting between two planar walls separated with a distance h, which can be obtained from eq. (15) for large distances, namely^{38,33}

$$\Pi_{\rm dl}(h) = \frac{2\sigma_+^2}{\varepsilon_0 \varepsilon} \cdot (2p_- - 1)e^{-2\kappa h} \tag{21}$$

The charged surface is denoted with subscript + and the neutral one with –. The corresponding surface charge densities are σ_+ and σ_- , whereby $\sigma_+ \neq 0$ and $\sigma_- = 0$. Both surfaces are further characterized with regulation parameters p_+ and p_- . Equation (21) is only correct for sufficiently large separations, but in this situation the pressure is simply proportional to the force acting between the two particles and also to their interaction energy.

This pressure originates from the compression of the diffuse layer formed near the charged interface by the neutral surface and has some unusual features. First, its decay length is half the Debye length. Second, its magnitude depends on the regulation parameter p_{-} of the neutral particle. In particular, for CP boundary conditions, where $p_{-}=0$, this force is attractive, while for CC boundary conditions, where $p_{-}=1$, this force is repulsive. Thus, depending on the regulation characteristics of the neutral surface, this pressure may become attractive or repulsive.

These features suggest the following dependence of the respective stability ratio for heteroaggregation on the ionic strength. For CP conditions, double layer forces are attractive, and thus they lead to a decrease of the stability ratio. This decrease is only modest, since the aggregation remains fast and diffusion controlled. For CC conditions, on the other hand, the double layer force is repulsive, and thus induces an increase of the stability ratio. Under these conditions, however, this increase is very pronounced, since a repulsive energy barrier forms, leading to slow and reaction limited aggregation. Equation (21) further suggests that for an intermediate regulation parameter $p_- = 0.5$, the stability ratio remains unity, as under these conditions the double layer interactions vanish.

These features can be quantitatively confirmed by means of respective calculations of the heterostability ratios, whereby the DH approximation given in eq. (21) was used. These results are shown as solid lines in Fig. 4. Indeed, CP conditions lead to a weak decrease of the heteroaggregation

stability ratio with decreasing ionic strength, while CC conditions lead to an abrupt increase of the stability ratio, and feature a CCC. For these calculations, the surface charge density of 10 mC/m^2 was used. This value represents the average of the magnitudes of the charge densities extracted from the electrophoretic mobilities by means of the standard electrokinetic model³⁹ and the PB charge-potential relationship for the isolated surface given in eq. (6). The actual charge densities are given in Table 2. Note that the results are independent of the sign of this charge. We have further used the particle radii of 150 nm and 120 nm for the charged and neutral particles, respectively. The Hamaker constant was chosen as 3.1×10^{-21} J. This value was used earlier in similar calculations^{34,40} and is close to values obtained from direct force measurements.^{41,42}

Since all experimentally measured stability ratios for heteroaggregation are below or close to unity, the comparison with the DLVO calculations demonstrate that the neutral particle surface must regulate close to CP conditions. While in this regime the dependence on the regulation parameter is weak, one can safely state that the regulation parameter must be below 0.5, and is probably close to zero. As detailed above, DLVO theory predicts major effects of charge regulation for heteroaggregation between charged and neutral particles. Based on the experimental heteroaggregation rates reported here it becomes possible to estimate an approximate value of the regulation parameter for the neutral surface. The charged-neutral case is thus the first situation described in the literature, where information on charge regulation can be obtained from measured aggregation rates.

So far we have implicitly assumed that the long-distance DH approximation given by eq. (21) correctly captures the trends in the stability ratio for heteroaggregation. Let us now present results from additional model calculations, which demonstrate that this claim remains correct within the more general Poisson-Boltzmann (PB) model and for a wider range of parameters.

These results are summarized in Fig. 5. First, one should realize that eq. (21) is exact within the DH approximation for $p_+ = 0.5$. Within the same approximation, the stability ratio is exactly unity, when regulation parameters for both surfaces are $p_+ = p_- = 0.5$. When the magnitude of the surface charge density is increased, the DH approximation fails, and the PB model must be used. These differences become appreciable for intermediate regulation conditions and charge densities near 10 mC/m^2 , see Fig. 5a. For the PB model, the double-layer forces become more repulsive, and the corresponding stability curves show an upturn and a well-defined CCC.

The effect of the charge density of the charged surface σ_+ is illustrated in Fig. 5b. While the influence of this quantity is important for CC and CR boundary conditions with $p_+ = p_- = 0.5$, its effect is minimal for CP boundary conditions. Moreover, charge regulation effects of the charged surface are small too. This feature is illustrated in Fig. 5c. On the other hand, the effect of charge regulation for the neutral surface is major, as already suggested by eq. (21), and further exemplified in Fig. 5d. In the

latter two sub-figures, the PB theory was used with a surface charge density of 10 mC/m^2 . When the regulation parameter is decreased, one observes a continuous transition from the CC to the CP situation. Initially, the stability ratio increases with decreasing ionic strength abruptly, and shows a corresponding CCC. This CCC progressively shifts to lower concentrations until it disappears, approximately for $p_- \le 0.4$. Below this value, one basically recovers the CP behavior. The above results were obtained for monovalent electrolytes, but additional PB calculations for asymmetric electrolytes demonstrate that the overall behavior basically remains the same. Equally, variations of the Hamaker constant and of the particle radii may induce shifts in CCCs, but close to CP conditions the behavior remains similar to the one discussed above.

These model calculations thus confirm that the simple force law given in eq. (21) captures the dependence of the stability ratio in the charge neutral case very well, particularly when the neutral surface regulates with $p_- \le 0.5$, and definitely near CP conditions. When charge regulation is less pronounced, the charge density of the charged particle and other parameters become relevant, but on the basis of the experimental data presented, this situation can be excluded with confidence.

Further evidence for CP conditions. The fact that neutral surfaces regulate close to CP conditions can be further verified by direct force measurements. Moazzami-Gudarzi et al. 43,44 have measured forces in solutions containing N6 and $K_4Fe(CN)_6$ between latex particles with the same amidine and sulfate functionalities, albeit of larger size. These systems behave similarly to the ones discussed here, and in particular the sulfate particles show a charge reversal in the presence of N6, while the amidine particles in the presence of the iron cyanide complexes. Force measurements are much more sensitive to the actual value of the regulation parameter, and from such experiments their values can be extracted with confidence. For the N6 system, minor variations of the respective regulation parameter with the N6 concentration was found, but the values lie between 0 and 0.15. For the $K_4Fe(CN)_6$ system, the regulation parameter was found to be near 0.07 and to be concentration independent. A related observation was made with the surface forces apparatus with highly charged mica and a gold electrode near the charge neutralization point. These authors report that the force profiles can be well explained when the gold surface is assumed to obey CP boundary conditions. Thus, direct force measurements independently confirm that neutral surfaces regulate close to CP conditions.

Another argument why a neutral surface is expected to behave close to CP conditions can be based on the expression for the regulation parameter given in eq. (7). The diffuse layer capacitance given in eq. (6) has a minimum for a neutral interface and its value at this minimum decreases with decreasing ionic strength. On the other hand, one may expect that inner capacitance is approximately independent of these parameters. Based on this argument one finds that the diffuse layer capacitance is much smaller than the inner one, and under these conditions the regulation parameter should be close to

zero. This argument again suggests that a neutral (or weakly charged) interface should regulate close to CP conditions.

Conclusion

Here we show for the first time that heteroaggregation process between charged and neutral particles is typically fast. This observation is based on a reanalysis of available experimental data and is confronted with calculations based on DLVO theory, which include effects of charge regulation. One finds that the neutral particles must regulate their surface charge strongly, likely close to the CP conditions. Such strong regulation behavior of neutral surfaces seems to apply quite generally to different systems, and is independently confirmed by direct force measurements. This charge regulation further follows by comparing the diffuse and inner layer capacitances of the interface. Should this behavior prove to be generally true, it provides a substantial simplification when dealing with heteroaggregation involving neutral particles.

At this point, however, one cannot exclude that in some systems a neutral surface would regulate its charge more weakly, or even behave close to constant charge (CC). In this situation, heteroaggregation processes would become highly sensitive to the charge regulation effects, and these effects would be much more important than those suggested here. To us it is unclear, however, whether such surfaces could be ever realized or found.

A further aspect that would require further study is the transition from the charge-neutral case discussed here to a pair of charged particles with different surface charge densities. In the former case, major effects of charge regulation are expected, while in the latter case, effects of charge regulation are likely to be small. The details of this transition are currently unknown, but would be worthwhile to investigate.

Acknowledgements

This work was supported by the Swiss National Science Foundation through awards 178759 and 159874 and the University of Geneva.

Table 1. Properties of the polystyrene latex particles used. 32,34

Abbreviation		AL	SL1	SL2
Mean particle radius (nm)	TEM ^a	151	300	125
	SLS b	149	297	117
	DLS^c	153	310	123
Polydispersity, coefficient of variation (%)	TEM ^a	5.7	2.2	3.1
Toryanspersity, esermerone or variation (%)	SLS b	6.5	3.0	7.2
Fast homoaggregation rate coefficient $(\times 10^{-18} \text{ m}^3/\text{s})^c$		2.8±0.2	3.1±0.3	2.8±0.2
CCC (M)		$0.15^d 0.25^e$	0.40^{e}	0.15^{d}

^aObtained by manufacturer by transmission electron microscopy (TEM). ^bMeasured by angle-resolved static light scattering. ^cMeasured by dynamic light scattering (DLS) at a scattering angle of 90°. ^{32,34} Homoaggregation rate coefficients obtained by time-resolved multi-angle dynamic light scattering in monovalent salt solutions. Extracted from the stability ratios measured by time-resolved dynamic light scattering at a scattering angle of 90° in ^dNaCl and ^eKCl solutions.

 Table 2. Properties of different charged-neutral systems investigated.

Additive	Concentration of additive (M)	Ionic strength (M)	Stability ratio for heteroaggregation ^a	Charge density (mC/m ²) ^b
N6 ^c	(7.0±0.5)×10 ⁻⁷	1.1×10 ⁻⁴	$0.56^{+0.08}_{-0.08}$	+2.7
	(1.25±0.05)×10 ⁻⁶	1.6×10 ⁻³	$0.70^{+0.08}_{-0.08}$	+6.8
	(1.05±0.06)×10 ⁻⁵	0.015	$0.82^{+0.10}_{-0.06}$	+16
	(1.1±0.1)×10 ⁻⁴	0.070	$0.96^{+0.10}_{-0.06}$	+21
K ₃ Fe(CN) ₆	(3.0±0.6)×10 ⁻⁴	1.9×10 ⁻³	$1.2^{+0.4}_{-0.2}$	-12
K ₄ Fe(CN) ₆	(1.0±0.1)×10 ⁻⁴	1.1×10 ⁻³	$0.9^{+0.6}_{-0.1}$	-8.4
OS^d	(4.0±0.3)×10 ⁻⁴	5.0×10 ⁻⁴	$1.1^{+0.5}_{-0.1}$	-8.3
	(4.4±0.4)×10 ⁻⁴	0.010	1.1 ^{+0.2} _{-0.1}	-8.4
	(6.4±0.6)×10 ⁻⁴	0.030	$1.2^{+0.2}_{-0.1}$	-8.6

^aSuperscripts and subscripts indicate asymmetric error bars obtained by error propagation from the standard deviations of the concentration of the additives at charge neutralization. ^bObtained from electrophoresis. The error is about 15%. ^cKCl and ^dNaCl used as background electrolyte.

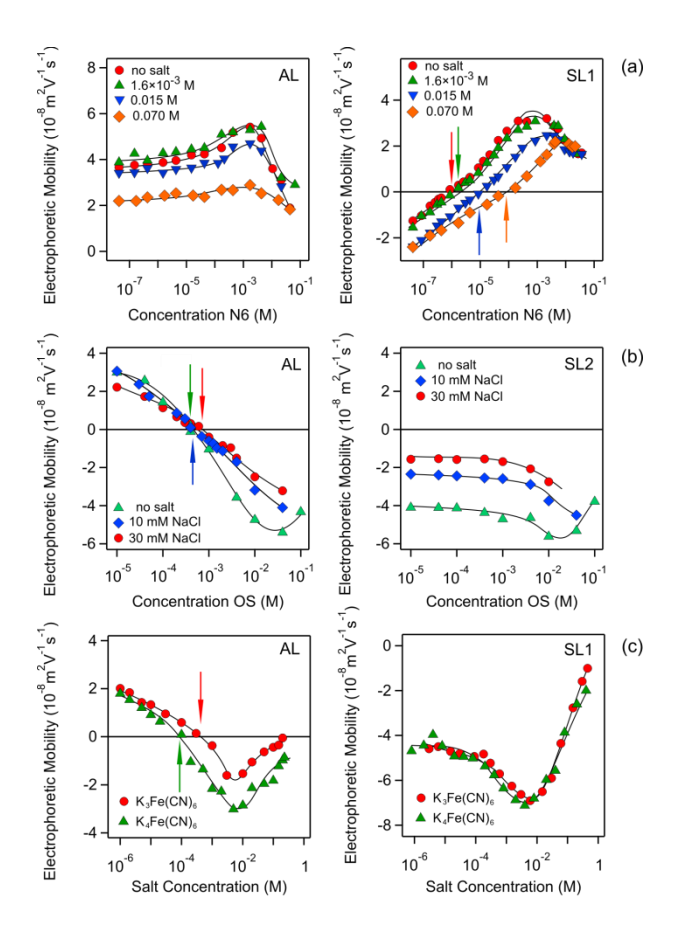


Figure 1. Electrophoretic mobility versus concentration of the respective additives at pH 4.0.^{32,34} Data for AL particles are shown in the left column, the ones for the SL1 and SL2 particles in the right one. Solid lines interpolate the data, and arrows indicate the charge reversal. (a) Aliphatic polyamine (N6) and (b) octylsulfate (OS) at different additions of monovalent salt. (c) Iron cyanide complexes with different charge.

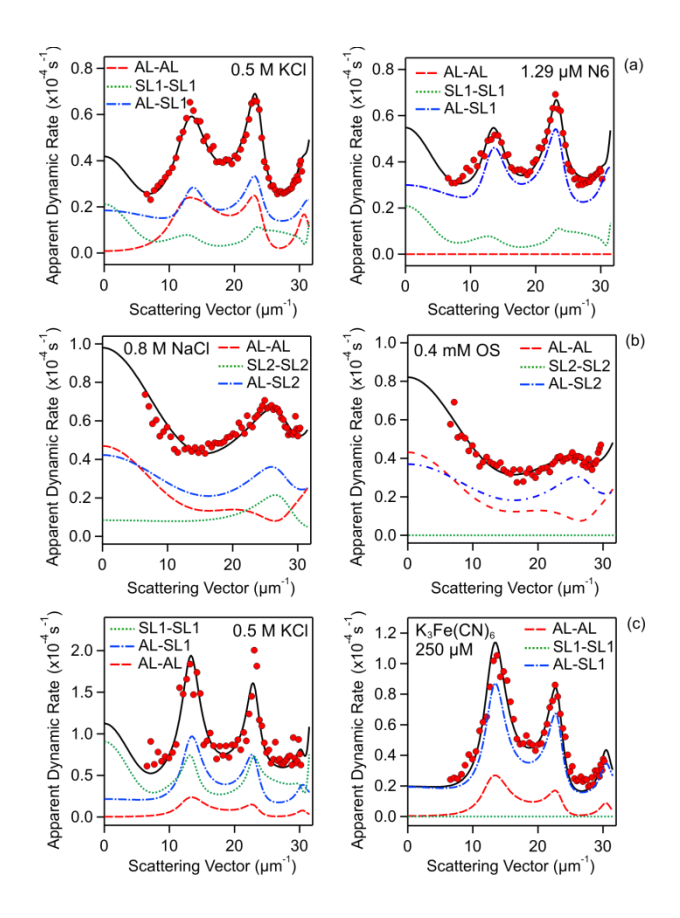


Figure 2. Apparent dynamic rates versus the magnitude of the scattering vector measured by time-resolved multi-angle light scattering. Statering and 2. Experimental data (points) are compared with best fits of the T-matrix theory (solid line). The contributions from the different aggregates are also indicated (broken lines). Data at high concentrations of monovalent electrolytes are shown in the left column, while the ones near the charge neutralization point in the right column. (a) AL and $SL1^{32}$, (b) AL and $SL2^{34}$, and (c) AL and $SL1^{32}$. The total particle concentrations and an AL particle number fractions are (a) 5.4×10^{13} m⁻³ and 0.74, (b) 6.6×10^{13} m⁻³ and 0.51, and 1.1×10^{14} m⁻³ and 0.42. The measured heteroaggregation rate coefficients at high concentrations of monovalent salt are (a,c) $(3.9 \pm 0.4) \times 10^{-18}$ m³/s and (b) $(3.1 \pm 0.2) \times 10^{-18}$ m³/s.

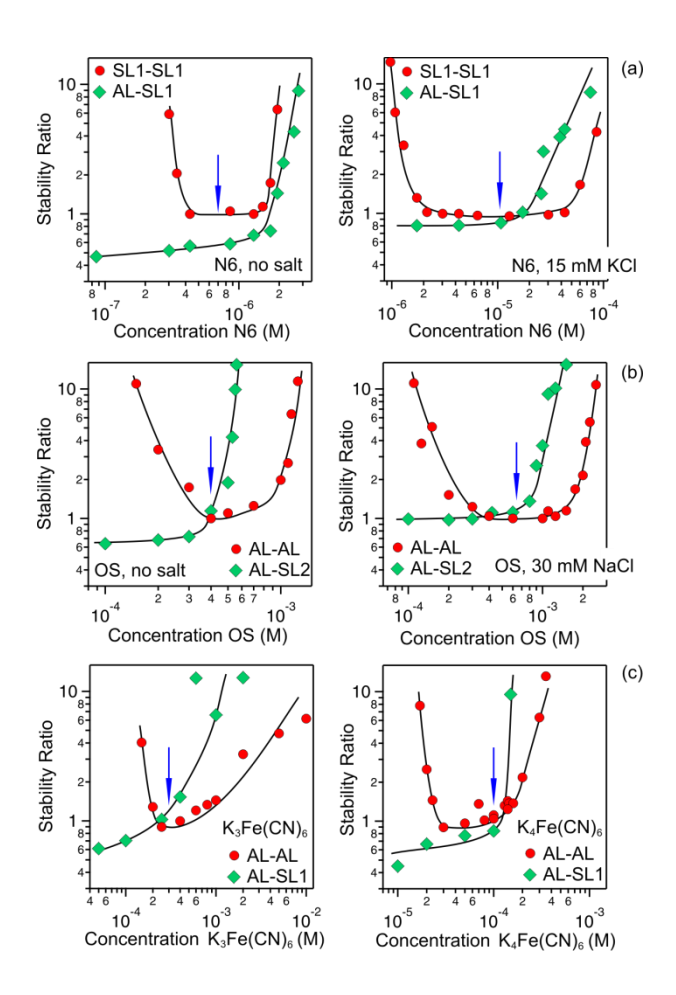


Figure 3. Stability ratios for heteroaggregation and homoaggregation near the charge neutralization point versus the concentration of the additives (a) N6 and (b) OS without (left) and with (right) added NaCl, and (c) iron cyanide complexes with different charge. The charge reversal points are indicated with arrows. The solid lines interpolate the experimental data.

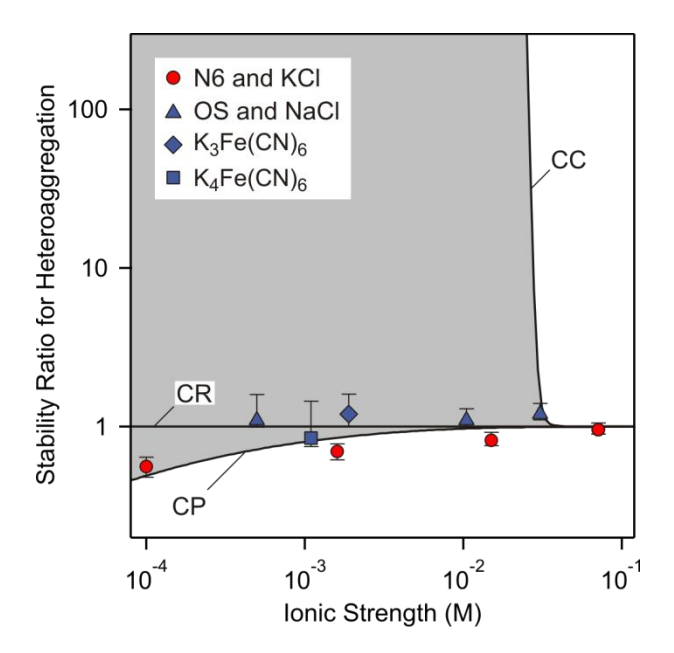


Figure 4. Comparison of experimental heteroaggregation stability ratios involving charged and neutral particles with calculations based on DLVO theory. These calculations were carried out for neutral particles with a radius of 120 nm, and charged particles with a radius of 150 nm and a surface charge density of 10 mC/m². The grey region is limited with the results for constant charge (CC) and constant potential (CP) boundary conditions.

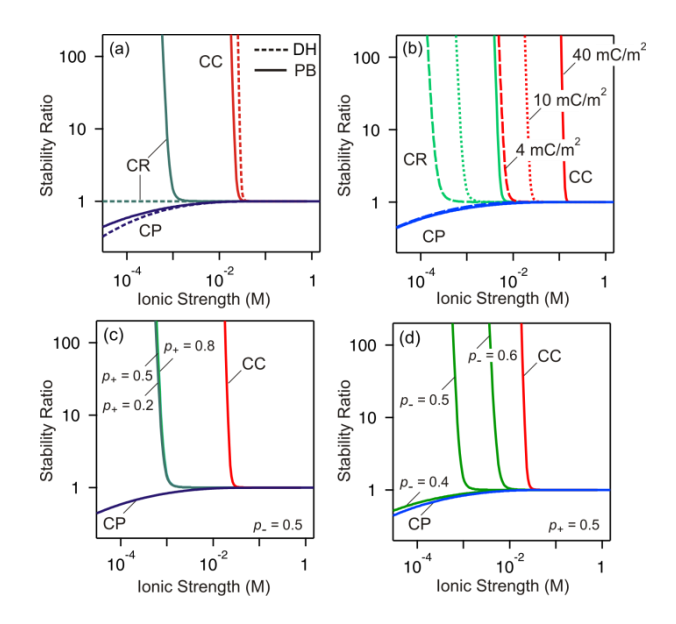


Figure 5. Results of DLVO calculations of stability ratios for heteroaggregation with different boundary conditions, namely constant charge (CC), constant potential (CP), and constant regulation (CR). (a) Comparison between DH (dashed) and PB (solid) approximations for a surface charge density of 10 mC/m². (b) Effect of the surface charge density σ_+ in the PB approximation. CR conditions use a regulation parameter of $p_+ = p_- = 0.5$ for both surfaces in (a,b). (c) Variation of the regulation parameter p_+ for the charged surface, while for the neutral surface $p_- = 0.5$ was kept fixed. (d) Variation of the regulation parameter p_- for the neutral surface, while for the charged surface $p_+ = 0.5$ was kept fixed.

References

- 1. Russel, W. B.; Saville, D. A.; Schowalter, W. R., *Colloidal Dispersions*. Cambridge University Press: Cambridge, 1989.
- 2. Elimelech, M.; Gregory, J.; Jia, X.; Williams, R. A., *Particle Deposition and Aggregation:*Measurement, Modeling, and Simulation. Butterworth-Heinemann Ltd.: Oxford, 1995.
- 3. Sandkuhler, P.; Lattuada, M.; Wu, H.; Sefcik, J.; Morbidelli, M., Further Insights into the Universality of Colloidal Aggregation. *Adv. Colloid Interface Sci.* **2005**, 113, 65-83.
- 4. Frens, G.; Heuts, J. J. F. G., The Double Layer Potential as a Rate Determining Factor in the Coagulation of Electrocratic Colloids. *Colloids Surf.* **1988**, 30, 295-305.
- 5. Tezak, B.; Matijevic, E.; Schulz, K. F., Coagulation of Hydrophobic Sols in Statu Nascendi 3. The Influence of the Ionic Size and Valency of the Counterion. *J. Phys. Chem.* **1955**, 59, 769-773.
- 6. Wiese, G. R.; Healy, T. W., Coagulation and Electrokinetic Behavior of TiO₂ and Al₂O₃ Colloidal Dispersions. *J. Colloid Interface Sci.* **1975**, 51, 427-433.
- 7. Behrens, S. H.; Christl, D. I.; Emmerzael, R.; Schurtenberger, P.; Borkovec, M., Charging and Aggregation Properties of Carboxyl Latex Particles: Experiments versus DLVO Theory. *Langmuir* **2000**, 16, 2566-2575.
- 8. Szilagyi, I.; Sadeghpour, A.; Borkovec, M., Destabilization of Colloidal Suspensions by Multivalent Ions and Polyelectrolytes: From Screening to Overcharging. *Langmuir* **2012**, 28, 6211-6215.
- 9. Chen, K. L.; Mylon, S. E.; Elimelech, M., Aggregation Kinetics of Alginate-Coated Hematite Nanoparticles in Monovalent and Divalent Electrolytes. *Environ. Sci. Technol.* **2006**, 40, 1516-1523.
- 10. Pavlovic, M.; Huber, R.; Adok-Sipiczki, M.; Nardin, C.; Szilagyi, I., Ion Specific Effects on the Stability of Layered Double Hydroxide Colloids. *Soft Matter* **2016**, 12, 4024-4033.
- Volodkin, D.; Ball, V.; Schaaf, P.; Voegel, J. C.; Möhwald, H., Complexation of Phosphocholine Liposomes with Polylysine: Stabilization by Surface Coverage versus Aggregation. *Biochim. Biophys. Acta* 2007, 1768, 280-290.
- 12. Balzer, B.; Hruschka, M. K. M.; Gauckler, L. J., Coagulation Kinetics and Mechanical Behavior of Wet Alumina Green Bodies Produced via DCC. *J. Colloid Interface Sci.* **1999**, 216, 379-386.
- 13. Farrokhpay, S., A Review of Polymeric Dispersant Stabilisation of Titania Pigment. *Adv. Colloid Interface Sci.* **2009**, 151, 24-32.
- 14. Barringer, E. A.; Bowen, H. K., High-Purity, Monodisperse TiO₂ Powders by Hydrolysis of Titanium Tetraethoxide 2. Aqueous Interfacial Electrochemistry and Dispersion Stability. *Langmuir* **1985**, 1, 420-428.

- 15. Xu, S. H.; Sun, Z. W., Progress in Coagulation Rate Measurements of Colloidal Dispersions. *Soft Matter* **2011**, 7, 11298-11308.
- 16. van Zanten, J. H.; Elimelech, M., Determination of Absolute Coagulation Rate Constants by Multiangle Light-Scattering. *J. Colloid Interface Sci.* **1992**, 154, 1-7.
- 17. Schneider, C.; Hanisch, M.; Wedel, B.; Jusufi, A.; Ballauff, M., Experimental Study of Electrostatically Stabilized Colloidal Particles: Colloidal Stability and Charge Reversal. *J. Colloid Interface Sci.* **2011**, 358, 62-67.
- 18. Puertas, A.; Maroto, J. A.; de las Nieves, F. J., Theoretical Description of the Absorbance Versus Time Curve in a Homocoagulation Process. *Colloids Surf. A* **1998**, 140, 23-31.
- 19. Derjaguin, B.; Landau, L. D., Theory of the Stability of Strongly Charged Lyophobic Sols and of the Adhesion of Strongly Charged Particles in Solutions of Electrolytes. *Acta Phys. Chim.* **1941,** 14, 633-662.
- 20. Verwey, E. J. W.; Overbeek, J. T. G., *Theory of Stability of Lyophobic Colloids*. Elsevier: Amsterdam, 1948.
- 21. Porubska, J.; Alince, B.; van de Ven, T. G. M., Homo- and Heteroflocculation of Papermaking Fines and Fillers. *Colloid Surf. A* **2002**, 210, 223-230.
- 22. Redman, J. A.; Grant, S. B.; Olson, T. M.; Estes, M. K., Pathogen, Filtration, Heterogeneity and the Potable Reuse of Wastewater. *Environ. Sci. Technol.* **2001**, 35, 1798-1805.
- 23. Mezzenga, R.; Schurtenberger, P.; Burbidge, A.; Michel, M., Understanding Foods as Soft Materials. *Nature Mater.* **2005**, 4, 729-740.
- 24. Rasa, M.; Philipse, A. P.; Meeldijk, J. D., Heteroaggregation, Repeptization and Stability in Mixtures of Oppositely Charged Colloids. *J. Colloid Interface Sci.* **2004**, 278, 115-125.
- 25. Ryde, N.; Matijevic, E., Kinetics of Heterocoagulation 4. Evaluation of Absolute Coagulation Rate Constants Using a Classical Light Scattering Technique. *J. Chem. Soc. Faraday Trans.* **1994,** 90, 167-171.
- 26. James, R. O.; Homola, A.; Healy, T. W., Heterocoagulation of Amphoteric Latex Colloids. *J. Chem. Soc. Farad. Trans. I* **1977**, 73, 1436-1445.
- Puertas, A. M.; Fernandez-Barbero, A.; de las Nieves, F. J., Induced Asymmetries in the Heteroaggregation of Oppositely Charged Colloidal Particles. *J. Colloid Interface Sci.* 2003, 265, 36-43.
- 28. Kihira, H.; Matijevic, E., Kinetics of Heterocoagulation 3. Analysis of Effects Causing the Discrepancy between the Theory and Experiment. *Langmuir* **1992**, 8, 2855-2862.
- 29. Lichtenfeld, H.; Shilov, V.; Knapschinsky, L., Determination of the Distance of Nearest Approach of Coagulated Particles in Haematite and Latex Dispersions. *Colloids Surf. A* **1998**, 142, 155-163.
- 30. Lopez-Lopez, J. M.; Schmitt, A.; Callejas-Fernandez, J.; Hidalgo-Alvarez, R., Cluster Discrimination in Electrostatic Heteroaggregation Processes. *Phys. Rev. E* **2004**, 69, 011404.

- 31. Lin, W.; Kobayashi, M.; Skarba, M.; Mu, C.; Galletto, P.; Borkovec, M., Heteroaggregation in Binary Mixtures of Oppositely Charged Colloidal Particles. *Langmuir* **2006**, 22, 1038-1047.
- 32. Cao, T.; Sugimoto, T.; Szilagyi, I.; Trefalt, G.; Borkovec, M., Heteroaggregation of Oppositely Charged Particles in the Presence of Multivalent Ions. *Phys. Chem. Chem. Phys.* **2017**, 19, 15160 15171.
- 33. Trefalt, G.; Montes Ruiz-Cabello, F. J.; Borkovec, M., Interaction Forces, Heteroaggregation and Deposition Involving Charged Colloidal Particles. *J. Phys. Chem. B* **2014**, 118, 6346-6355.
- 34. Cao, T.; Trefalt, G.; Borkovec, M., Measuring Slow Heteroaggregation Rates with Time-Resolved Multi-Angle Dynamic Light Scattering. *J. Colloid Interf. Sci.* **2020**, 566, 143-152.
- 35. Mishchenko, M. I.; Mackowski, D. W., Electromagnetic Scattering by Randomly Oriented Bispheres: Comparison of Theory and Experiment and Benchmark Calculations. *J. Quant. Spectrosc. Radiat. Transf.* **1996**, 55, 683-694.
- 36. Mishchenko, M. I.; Travis, L. D.; Lacis, A. A., *Scattering, Absorption, and Emission of Light by Small Particles* University Press: Cambridge 2002.
- 37. Yu, W. L.; Matijevic, E.; Borkovec, M., Absolute Heteroaggregation Rate Constants by Multiangle Static and Dynamic Light Scattering. *Langmuir* **2002**, 18, 7853-7860.
- 38. Carnie, S. L.; Chan, D. Y. C., Interaction Free Energy between Plates with Charge Regulation: A linearized model. *J. Colloid Interface Sci.* **1993**, 161, 260-264.
- 39. O'Brien, R. W.; White, L. R., Electrophoretic Mobility of a Spherical Colloidal Particle. *J. Chem. Soc. Farad. Trans. II* **1978**, 74, 1607-1626.
- 40. Cao, T.; Trefalt, G.; Borkovec, M., Aggregation of Colloidal Particles in the Presence of Hydrophobic Anions: Importance of Attractive Non-DLVO Forces. *Langmuir* **2018**, 34, 14368-14377.
- 41. Moazzami-Gudarzi, M.; Trefalt, G.; Szilagyi, I.; Maroni, P.; Borkovec, M., Forces between Negatively Charged Interfaces in the Presence of Cationic Multivalent Oligoamines Measured with the Atomic Force Microscope. *J. Phys. Chem. C* **2015**, 119, 15482-15490.
- 42. Smith, A. M.; Maroni, P.; Borkovec, M., Attractive Non-DLVO Forces Induced by Adsorption of Monovalent Organic Ions. *Phys. Chem. Chem. Phys.* **2018**, 20, 158-164.
- 43. Moazzami-Gudarzi, M.; Trefalt, G.; Szilagyi, I.; Maroni, P.; Borkovec, M., Nanometer-Ranged Attraction Induced by Multivalent Ions between Similar and Dissimilar Surfaces Probed by the Atomic Force Microscope (AFM) *Phys. Chem. Chem. Phys.* **2016**, 18, 8739-8751.
- Moazzami-Gudarzi, M.; Adam, P.; Smith, A. M.; Trefalt, G.; Szilagyi, I.; Maroni, P.; Borkovec,
 M., Interactions between Similar and Dissimilar Charged Interfaces in the Presence of
 Multivalent Anions. *Phys. Chem. Chem. Phys.* 2018, 20, 9436-9448
- 45. Tivony, R.; Ben Yaakov, D.; Silbert, G.; Klein, J., Direct Observation of Confinement-Induced Charge Inversion at a Metal Surface. *Langmuir* **2015**, 31, 12845-12849.